Journal of Catalysis **210,** 198–206 (2002)
doi:10.1006/jcat.2002.3678

A DFT Study on CO Oxidation over Co_3O_4

Peter Broqvist,*,† Itai Panas,‡,[1] and Hans Persson*,†

*Department of Applied Physics, Chalmers University of Technology, SE-412 96 Göteborg, Sweden; †Competence Centre for Catalysis, Chalmers University of Technology, SE-412 96 Göteborg, Sweden; and ‡Department of Inorganic Environmental Chemistry, Chalmers University of Technology, SE-412 96 Göteborg, Sweden

Received February 13, 2002; revised May 8, 2002; accepted May 8, 2002

A pilot investigation regarding the CO oxidation mechanism at the Co_3O_4(110) surface is performed by means of first-principles calculations based on density functional theory. Preferred adsorption of CO is found to occur at a surface Co^{3+} site. A possible mechanism for CO_2(g) formation of the Mars–van Krevelen type is also looked into via the monitoring of two inequivalent oxygen abstraction routes. Experimental observations regarding partial surface deactivation are discussed based on surface intermediates. The oxidative property of the Co_3O_4 substrate, i.e., $Co^{3+} + e^- \rightarrow Co^{2+}$, is found to be crucial for the O abstraction step. This implies that $CoAl_2O_4$ is inactive in CO oxidation, in agreement with experiment.

1. INTRODUCTION

Environmental catalysis implies employing a catalyst to convert unwanted emissions from, for example, combustion engines into harmless compounds. However, before the catalyst has been heated to the light-off temperature, the emissions are released untreated into the atmosphere. In fact, about 80–90% of all harmful emissions are released during this cold start stage (1, 2). The present study seeks to contribute to the understanding of the catalytic oxidation of hydrocarbons, i.e.,

$$C_xH_y + (x + y/4)O_2(g) \rightarrow x\,CO_2 + y/2\,H_2O, \quad [1]$$

where O_2(g) is the reactant to be activated. Commonly, noble metals such as platinum are employed, since O_2(g) is known to react with such metals to form a surface oxygen O_2^-(ads) phase (3), which in turn oxidizes the hydrocarbons. However, at low temperatures carbon monoxide adsorption on Pt has been shown to hinder oxygen loading, thus effectively poisoning the catalyst.

Several suggestions exist about how to improve catalyst performance during cold starts. One strategy employs a closed-coupled catalyst, meaning that the catalyst is placed close to the engine in order to exploit the higher exhaust gas temperature at this location. A second alternative involves hydrocarbon traps, which absorb the hydrocarbons during the heating of the catalyst (4). This study addresses a third approach, which contributes to the search for catalysts that display high activity for the oxidation of hydrocarbons at low temperatures. The difficulty lies in identifying a material which fulfils all the requirements of an efficient catalyst; meaning that in addition to the above, the catalyst should also exhibit high stability towards poisoning at low temperatures, and high stability towards thermal deactivation at elevated temperatures. Such materials are commonly sought among the oxides of the transition metals, since the ability of the metal ions to display several metastable oxidation states would produce reactive oxides towards both hydrocarbon and CO(g) oxidation. In this context, the heterogeneous CO oxidation reaction is commonly used as a probe for the low-temperature activity of possible catalytic materials. Several such materials have been found to be efficient for CO(g) oxidation at low temperatures. In particular, Co_3O_4(s) has been shown to display catalytic activity for CO(g) oxidation down to -60°C by Thormählen *et al.* (5), and similar results have been reported by other research groups (6–10) as well.

The interactions of CO(g) with Co_3O_4(s) at low temperatures are of interest on several accounts. First, this substrate is known to be the most active oxide among the base metal oxides in the first-row transition metal series for the catalysis of oxygen-transfer reactions at low temperatures (11, 12). Second, it is possible to experimentally study CO(g) oxidation on *pure* Co_3O_4(s), implying that the complex interactions with any support material or impurity are absent, which in turn simplifies the evaluation of the experiments. Generally, CO(g) oxidation on transition metal oxides follows a mechanism proposed by Mars–van Krevelen (13), which implies that lattice oxygen is found in the resulting CO_2(g) reaction product. Support for this mechanism is also found in the case of CO(g) oxidation on Co_3O_4/Al_2O_3 by means of isotope experiments (14).

Major drawbacks for employing Co_3O_4(s) as catalyst involves deactivation (a) in a $CO(g) + O_2(g)$ atmosphere

[1] To whom correspondence should be addressed. E-mail: itai@inoc.chalmers.se.

0021-9517/02 $35.00

(14), (b) by common gases like water, and (c) by solid-state reaction, with the most common catalyst support, Al_2O_3, forming the inactive $CoAl_2O_4$(s) compound (15). Few studies are found in the literature on the detailed surface chemistry of Co_3O_4(s). The complex spinel structure of the Co_3O_4(s) makes it difficult to identify the active sites of, for example, the oxidation mechanism. Such knowledge is needed, however, as it could later be used in the design of novel low-temperature-active catalytic composite materials, which are more resistant towards poisoning and deactivation. Iwasawa (16) discusses the possible adsorption and oxidation mechanism of CO(g) at $[Co_3O_4]_n$ clusters, which display the inherent raft-like nano structures, present at the (110) surface. It is in this context that the present work aims to contribute, that is, by formulating mechanisms for the CO(g) oxidation on the ideal (110) surface of Co_3O_4(s).

The present theoretical investigation employs first-principles calculations based on density functional theory in order to address this CO(g) oxidation reaction on Co_3O_4(s). In the past few years *first-principle* calculations based on Kohn–Sham density functional theory (17) have garnered much interest among solid-state physicists and chemists. This was initially due to the success of the *local density approximation* (LDA), which was originally intended for solids with spatially slowly varying electronic densities. Still, the method has proved useful for estimating properties of gas-phase molecules and molecular adsorbates. Improvements in the descriptions of the density functional in terms of gradient corrections and nonlocal correlation effects have resulted in a powerful tool for addressing also such strongly inhomogeneous electronic densities as those found in molecules, semiconductors, and insulator surfaces. In the present DFT study we use the generalised gradient approximation (GGA) in the spin-polarised Perdew–Burke–Ernzerhof exchange-correlation description (PBE) (18) to overcome the most problematic deficiency of LDA: the large overbinding of atoms.

This study addresses, first, the applicability of the pseudopotential approximations within the chosen density functional by computing relevant structural properties for bulk Co_3O_4(s), and the stability of the (110) surface of this oxide. Second, possible CO(g) oxidation sites at the (110) surface are compared, employing the molecule as a probe. Third, reaction channels for formation of CO_2(g) are investigated and a possible reaction mechanism for the CO(g) oxidation is discussed. Particularly, an explanation is arrived at as to why the apparent analogue to Co_3O_4(s), i.e., $CoAl_2O_4$(s), is inactive towards CO(g) oxidation.

2. THEORY AND METHODS

The calculations performed in this study were done using the commercial version of the software package CASTEP (Cambridge Sequential Total Energy Package) (19) inside Cerius^2 (20). This method evaluates by means of density functional theory the total energy of periodically repeating supercells. The pseudopotential approximation is employed, replacing the inert core regions of the atoms. Thus only the valence electrons are treated explicitly in the calculations, while the core–valence interaction is described by pseudopotentials. Periodic boundary conditions are used, with the electronic orbitals expanded in a plane–wave basis. The expansion includes all plane waves whose kinetic energy satisfies $\hbar^2k^2/2m < E_{cut}$, where k is the wave vector, m is the electronic mass, and E_{cut} is the chosen cutoff energy. The Brillouin zone was sampled with the Monkhorst–Pack scheme (21). For the approximation of the exchange-correlation energy, a generalised gradient-corrected spin-polarised functional was used as proposed by Perdew *et al.* (18). This functional is the GGS–PBE. It was previously shown that the gradient-corrected approximation improves greatly on the energetics of molecular adsorption compared to that of the local density approximation (LDA) (22).

In this study we used nonlocal ultrasoft pseudopotentials, as proposed by Vanderbildt (23). These potentials are accessed from the CASTEP database (19). Briefly, the 1s-2p states of Co as well as O 1s are treated as core states. When automatic geometry optimisation was performed, the concerted scheme for electronic and geometry optimisation by Fischer and Almlöf (24) was employed.

3. RESULTS AND DISCUSSION

The results include a test of the computational method (cf. Section 3.1), the search of adsorption sites for CO on the Co_3O_4(110) surface (cf. Section 3.2), and a comparison of two reaction channels for CO_2 formation (cf. Section 3.3), and finally a possible mechanism for the CO-oxidation reaction is proposed.

3.1. Validation of Computational Approach

A number of tests were initially performed to verify the accuracy of the method when applied to bulk Co_3O_4, to the (110) surface, and to the isolated sorbates CO and CO_2. The parameters were the choice of cutoff energy and the k-point sampling.

The geometry optimisations performed on Co_3O_4 indicate that a good agreement between predicted and experimental structure (25) is obtained at a cutoff energy of 260 eV and a k-point spacing of 0.05 Å^{-1}. The surface site geometry was obtained by cleaving the solid in the (110) normal direction, thus obtaining the 8.17 Å × 5.79 Å surface unit cell. The results for the relaxation of the Co_3O_4(110) surface modelled as an infinite stack of three-layer slabs with a fixed bottom layer separated by a 10-Å vacuum layer indicate no significant displacement of the surface atoms along the (110) direction. This vacuum width was deemed sufficient also for the CO adsorption calculations due to the fact

TABLE 1

Comparing Predicted Structures and Model Reaction Enthalpies for the Functionals GGS–PBE[a] and B3LYP

	GGS–PBE		B3LYP	Experiment
	260 eV	380 eV	6-311G(d,2pd)	(Ref.)
Co_3O_4 spinel				
Co^{+III}–O^{-II}	1.95 Å	1.95 Å		1.916 Å (25)
Co^{+II}–O^{-II}	1.94 Å	1.95 Å		1.942 Å (25)
a	8.17 Å	8.19 Å		8.083 Å (25)
CO				
C–O	1.14 Å	1.14 Å	1.13 Å	1.128 Å (26)
CO_2				
C–O	1.17 Å	1.17 Å	1.16 Å	1.160 Å (26)
H_2				
H–H	0.75 Å	0.75 Å	0.74 Å	0.741 Å (26)
H_2O				
H–O	0.97 Å	0.97 Å	0.96 Å	0.958 Å (26)
Λ(H–O–H)	105.07°	105.18°	103.84°	104.51° (26)
$CO_2 + H_2 \rightarrow CO + H_2O$				
ΔE	−0.764 eV	−0.879 eV	−0.602 eV	
			−0.729[b] eV	−0.427 eV (26)

[a] Data for two different cutoff energies are reported in the case of GGS–PBE.

[b] Vibrationally zero-point-corrected enthalpy.

that CO adsorption energy does not significantly change by increasing this interslab distance. This result may also be taken to infer the effective absence of any artificial attractive interslab-induced dipole-induced dipole interactions. Lateral adsorbate–adsorbate interaction is understood to represent what is expected for an intermediate-to-high-coverage situation.

Calculations performed on the isolated CO and the isolated CO_2 molecule were found to be in good agreement with the experimental bond lengths (26) for the 260-eV cutoff energy. Reaction energetics for the model oxygen abstraction reaction

$$H_2 + CO_2 \rightarrow H_2O + CO \qquad [2]$$

was considered in order to substantiate the applicability to relevant chemistry of the 260-eV cutoff in the CASTEP/GGS–PBE procedure. Thus, comparisons of the results for the 260- and 380-eV cutoff energies were made. The consistency among gradient-corrected functionals in predicting reaction enthalpies was tested by comparing the GGS–PBE results to those obtained by the B3LYP hybrid functional (27–30), the latter employing the 6-311G(d,2pd) basis set to the above-mentioned model reaction. The computed data together with the experimental values for bond lengths are given in Table 1. These results are taken as support for the computational procedure employed in the present study.

3.2. CO Adsorption on the Co_3O_4(110) Surface

The potential energy surface for adsorption of CO was scanned by means of single-point total energy calculations. The adsorption energy was calculated according to the expression

$$E_{ads} = E_{CO+slab} - E_{CO} - E_{slab}, \qquad [3]$$

where E_{CO} is the single-point energy of the isolated CO molecule in its equilibrium configuration and E_{slab} is the calculated single-point energy of the slab configuration used. A negative E_{ads} corresponds to a stable adsorbate/slab system.

Adsorption energy curves were computed with respect to site-to-carbon distance. The first candidate site involves a Co^{3+} ion in a subatomic layer (Section 3.2.1). The second adsorption configuration considered is a surface Co^{3+} ion (Section 3.2.2). Section 3.2.3 discusses the nature of the formed Co^{3+}–CO bond.

3.2.1. CO adsorption on a subatomic-layer Co^{3+} ion. In Fig. 1, the active site discussed by Iwasawa (16) is displayed. This site has a cobalt(III) ion in the second atomic layer, and two nearest-neighbouring oxygen atoms in the surface layer. Upon the approach of the CO molecule to this site, and based on the results from the calculations shown in Table 2 it is suggested that Pauli repulsion to these oxygen ions, renders this site inaccessible. Support for this interpretation is found from calculations performed on a CO molecule approaching the surface oxygen atoms directly, as these display similar repulsions. It is concluded that access

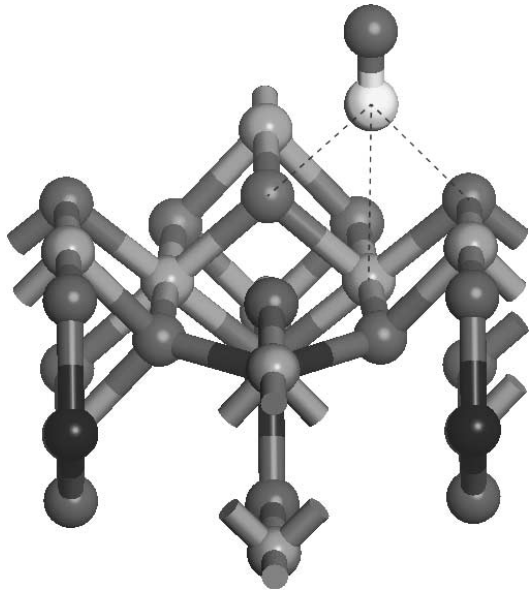

FIG. 1. Adsorption on a sublayer Co^{3+} ion. Note how the adsorption becomes sterically hindered (cf. Table 2) because there is little space between the surface oxygen ions where CO enters. Dark grey, oxygen; light grey, Co(III); black, Co(II); and white, carbon.

TABLE 2

Potential Energy Scan from Single-Point Energy Calculations; Adsorption of CO on Co^{+III} at a *Sublayer Site*[a]

$R[Co^{3+}–CO]$ (Å)	E_{ads} (eV)
1.52	5.27
2.34	1.45
2.80	0.93
3.04	0.65

[a] Positive numbers correspond to repulsive configurations.

TABLE 3

Potential Energy Scan from Single-Point Energy Calculations; Adsorption of CO on Co^{+III} at a *Top-Layer Site*[a]

$R[Co^{3+}–CO]$ (Å)	E_{ads} (eV)
1.30	3.68
1.50	−0.26
1.80	−1.76
2.00	−1.52
2.52	−0.53

[a] Positive numbers correspond to repulsive configurations.

to this Co(III) site is sterically hindered, which effectively rules out this site for CO adsorption on an ideal Co_3O_4(110) surface.

3.2.2. CO adsorption on a top-layer Co^{3+} ion. Here, the CO molecule approaches an exposed surface cobalt(III) ion. The site is depicted in Fig. 2, where the CO molecule is found to adsorb with the carbon pointing to the surface as it binds to the Co^{3+} site. The results from these calculations are shown in Table 3. The minimum on the potential energy curve is found at $R_{C–Co(III)} = 1.8$ Å. The binding energy becomes 1.7 eV. Scanning the potential energy surface by single-point calculations was also perfomed. By rotating the CO molecule 180° ($R_{O–Co(III)} = 2.0$ Å) the adsorption energy becomes only 0.5 eV, while for the 135° rotation, a binding energy of 1.0 eV ($R_{C–Co(III)} = 1.8$ Å) is obtained. These results are taken to imply that the CO molecule adsorbs on the exposed cobalt(III) surface site with the carbon end towards the surface and the molecular axis parallel to the surface normal direction (cf. Fig. 2).

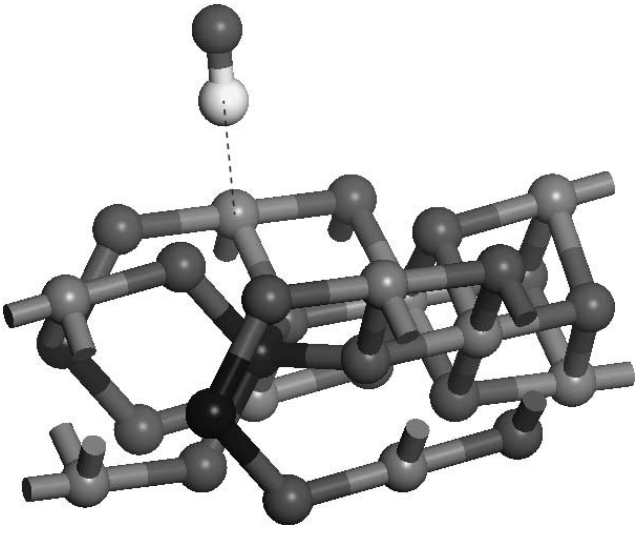

FIG. 2. Molecular CO adsorption at a surface exposed cobalt(III) ion. This is the only favourable site found for CO adsorption (cf. Table 3).

3.2.3. Effects on magnetic properties due to bonding. The ground-state low-spin cobalt(III) $3d^6$ electronic configuration, resulting from the octahedral ligand field, is well documented (31). It is illustrated in Fig. 3, and it is consistent with our calculations on the bare Co_3O_4 (110) surface.

When the CO molecule approaches the surface, a distinct change in the properties of the system is found to occur at $R_{C–Co(III)} \approx 2$ Å. The total spin density increases, which indicates a distortion of the ligand field experienced by Co(III), i.e., the CO molecule 5σ lone pair interacts with one of the doubly occupied cobalt 3d orbitals of local t_{2g} symmetry. Thus, the t_{2g} orbital degeneracy is partly lifted, as Pauli repulsion with the CO 5σ orbital brings one of these 3d orbitals closer to the empty e_g subspace. Thus three orbitals become near-degenerate (see Fig. 4), and the same effects which are responsible for Hund's rule can be employed to understand the preference for the high-spin state. Thus, the present study predicts that initial CO adsorption on the Co_3O_4(110) surface will cause a diamagnetic-to-paramagnetic surface transition.

The nature of the CO to cobalt(III) ion bond is understood from the minor (0.01 Å) relaxation of the intramolecular C–O bond distance upon adsorption, in conjunction with the substantial adsorption energy (1.7 eV). Taken together, these results imply that chemisorption results solely from the 5σ lone-pair dative bonding to the Co(III) ion, i.e., no backdonation from the cobalt ion 3d space to the π^*

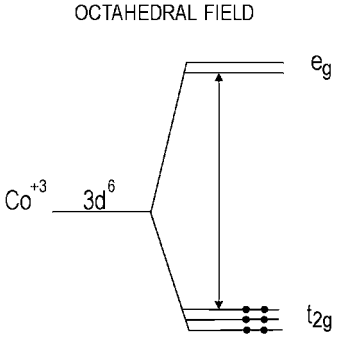

FIG. 3. Spin configuration for Co^{3+} in an octahedral ligand field.

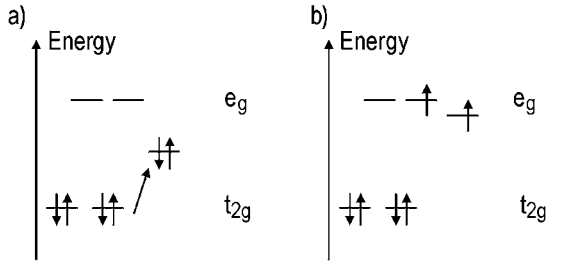

FIG. 4. (a) One of the t_{2g} energy levels involved in the CO adsorption becomes destabilised due to symmetry lowering, resulting from the adsorption. (b) A transition from diamagnetic to paramagnetic Co(III) occurs due to the reduced energy splitting between the two original e_g orbitals and one of the t_{2g} components.

orbital of CO occurs. This is as expected, given the high (3+) formal charge of Co(III). Effectively, this bonding situation results in a slightly positive adsorbate, as the 5σ lone pair is to some extent shared with the Co(III) ion.

3.3. Two Reaction Channels for CO_{ads} to CO_2(g) Formation

It was shown in Section 3.2.2, that the initial reactive CO adsorption occurs at the exposed Co(III) site on the (110) surface of Co_3O_4(s). The two simplest reaction channels for CO_2 formation, by the Mars–van Krevelen mechanism, involve the two adjacent surface oxygen ions. These two surface oxygen ions differ in the way they are bonded in the structure. A top view of the active site is depicted in Fig. 5. These (110) surface oxygen ions differ in that one is bonded to one Co(II) ion and one Co(III) ion, while the second O_{surf} has three Co(III) ions as nearest neighbours. Thus, the two surface oxygen ions experience different crystal fields, which causes their electropositivities to differ, and thereby also their reactivities. These oxygen ions are hereafter indicated O_W and O_S, representing the weaker and stronger local crystal field sites, respectively. The two issues addressed in this section concern (a) whether one or both of the mentioned oxygen ions can be employed to produce CO_2, and (b) characteristics of the corresponding reaction paths for CO_2 formation. Thus, Section 3.3.1 addresses the exit channels where the CO_2 product is assumed to have formed. Section 3.3.2 scans the corresponding reaction paths, while in Section 3.3.3 implications based on these results are discussed.

3.3.1. Two exit channels. The CO_2 product, resulting from CO oxidation, may produce two different surface oxygen vacancies dependent on whether O_W or O_S is abstracted, in accord with the experimentally verified Mars–van Krevelen mechanism. The stability of the reduced substrate decides its electron-buffering capacity and to what extent it can be useful as an oxidation agent. In this section, we assume the formation of the CO_2 molecule to have already occurred. We determine the relative stabilities for the two situations and compare the two potential energy curves (PEC). The PEC are scanned by means of single-point DFT calculations at different distances between each of the vacancies and the CO_2 molecule, as indicated in Fig. 6. Thus the number of atoms and the total number of electrons in the system are conserved throughout the calculations. The exit channel of the CO oxidation mechanism in the case of O_W abstraction displays a potential energy curve with an outer (−2.5 eV) and an inner (−1.8 eV) energy minimum (cf. Fig. 7) corresponding to the CO_2 and the formal CO_2^{2-} species, respectively. The potential energy curves' crossing occurs at 0.5 Å from the original oxygen lattice position. The existence of a formal CO_2^{2-} intermediate of significant

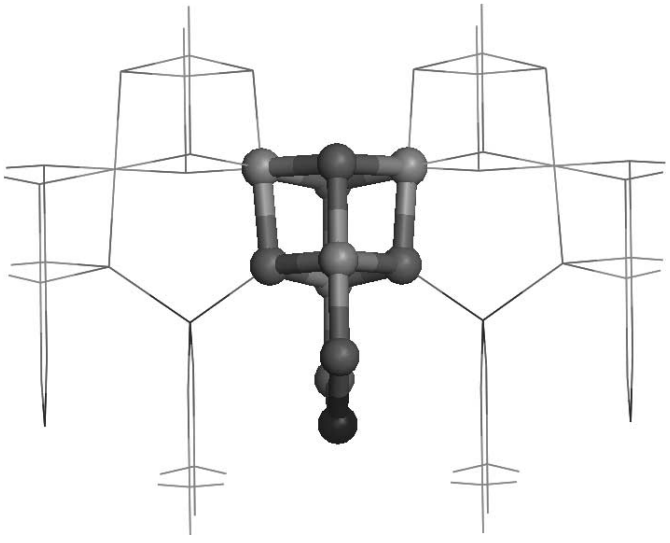

FIG. 5. A ball-and-stick model on the active site employed for CO adsorption and continuous CO oxidation, according to the Mars–van Krevelen mechanism.

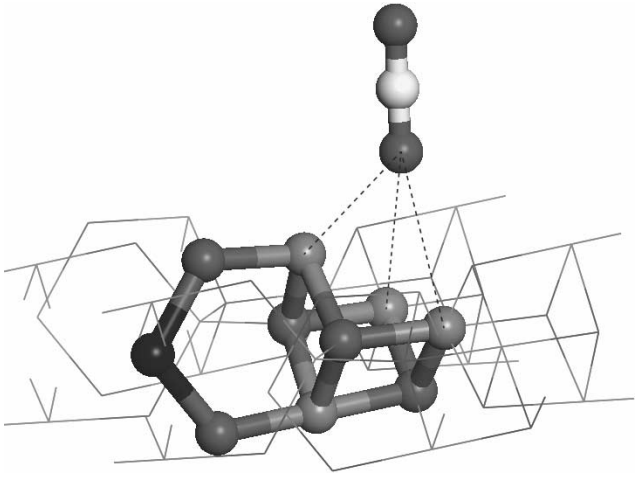

FIG. 6. Oxygen (O_S) abstraction from the surface to form CO_2 is schematically depicted.

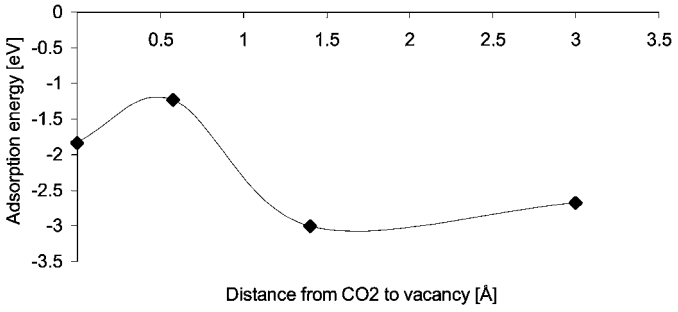

FIG. 7. Results from single point energy calculations for the abstraction of the oxygen experiencing the weaker crystal field (O_W). A linear CO_2 molecular product arrangement is employed as probe.

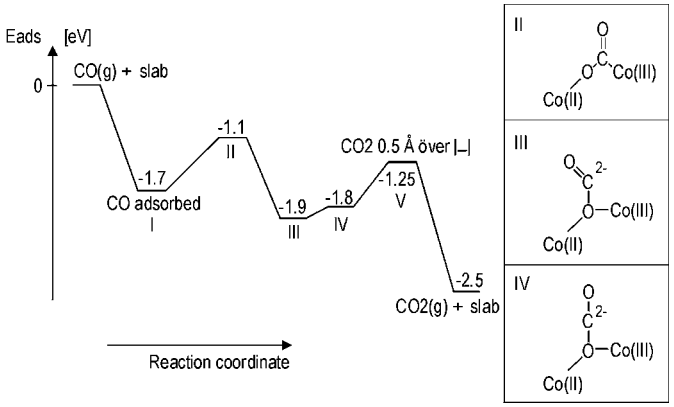

FIG. 9. An overall energy diagram for reaction pathway A is shown. Notice the energy barrier upon CO_2 leaving the surface. Simplified sketches for the intermediates are shown to the right. The |_| pocket denotes oxygen vacancy O_W.

stability (local minimum on the PEC) reflects the weakness of the local crystal field at the O_W site. Such a local minimum on the PEC is not found at the O_S site (cf. Fig. 8) because of the strong electron affinity of this site. The relative stabilities of the asymptotes, 2.5 and 1.6 eV in case of O_W and O_S removal, respectively, are taken to reflect the reducing power of the excess electrons at the O_S site. Indeed, removal of O from the O_W site results in a more efficient reduction of the surface Co(III) ions than does removal of O from the O_S site. Furthermore, it is noted that O abstraction from O_S (Fig. 8) displays stability similar to that of the initial Co(III)–CO species (Table 3), while O abstraction from O_W (Fig. 7) produces a significantly more stable product. This property is expected to affect in a significant way the nature of the Co_3O_4 surface at thermodynamic equilibrium in the presence of CO(g).

3.3.2. Two overall reaction pathways. Subsequent to investigating the entrance channel in Section 3.2, and the exit channels for the O_W and O_S abstractions in Section 3.3.1, the stabilities of the intermediate surface transients are addressed here. The configurations and corresponding energetics are displayed in Figs. 9 and 10. It is noted that for the O_W channel (Fig. 9) all points on the schematic potential energy curves lie well below the CO(g) + slab starting point, while, in contrast, intermediate states on the O_S abstraction path approach zero stability for the same reference point.

The two pathways may be summarised as follows:

1. *O_W abstraction pathway.* This reaction involves the surface oxygen which experiences the weaker crystal field (O_W). The stabilities at stages I–V in Fig. 9 correspond to the following:

Stage I. Adsorption of CO on the active cobalt(III) site occurs, with the CO molecule adsorbing straight at a distance of 1.8 Å above the Co^{3+} ion.

Stage II. Formation of a bent CO_2^{-2} species occurs as the carbon monoxide molecule glides towards O_W. The structure of this charged transient surface CO_2 species results from CO bridging the Co(III) and O_W sites. Here, the orbital hybridisation on the carbon resembles that of the formaldehyde molecule.

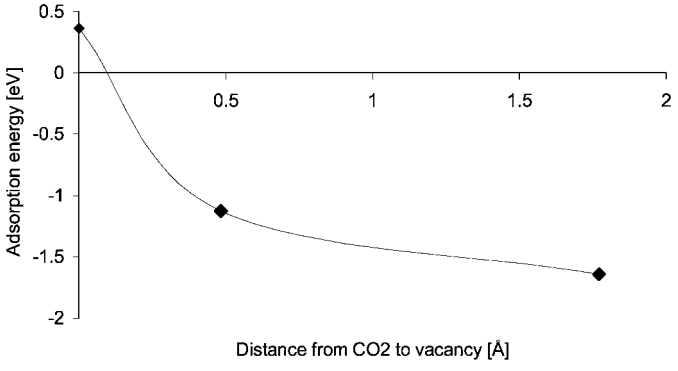

FIG. 8. Results from single point energy calculations for the abstraction of the oxygen experiencing the stronger crystal field (O_S). A linear CO_2 molecular product arrangement is employed as probe.

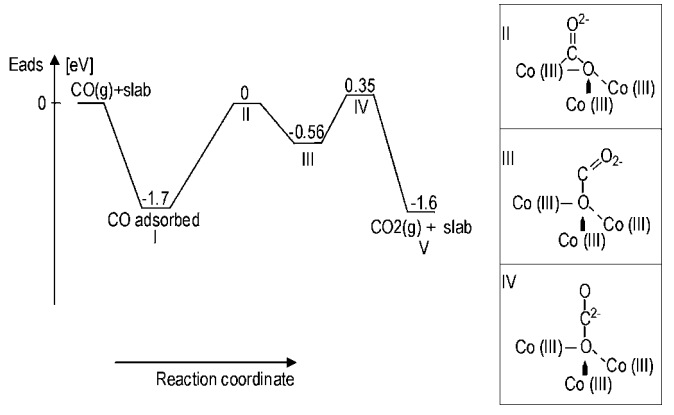

FIG. 10. An overall energy diagram for reaction pathway A is shown. Simplified sketches for the intermediates are shown to the right. The |_| pocket denotes oxygen vacancy O_S.

Stage III. Upon dissociation of the Co(III)–C bond, Pauli repulsion causes the O_W–C bond to become parallel to the surface normal. The resulting surface CO_2 species stays bent, as it remains a formally doubly charged anion.

Stage IV. The charged triatomic molecule straightens along a normal coordinate, which becomes the reaction coordinate, and the linear CO_2 species displays a quasistable structure on the potential energy surface.

Stage V. Desorption occurs by surmounting an energy barrier associated with the reduction of the substrate. The existence of two potential energy minima reflects the metastable nature of this reduced substrate site. Excess electrons are either shared with the CO_2 molecule or dispersed into the slightly distant neighbouring Co(III) sites. The asymptotic stability for CO_2 + reduced O_W site becomes 2.5 eV.

2. *O_S abstraction pathway.* This reaction path involves the surface oxygen which experiences the stronger crystal field (O_S). The stabilities for the steps I–V are shown in Fig. 10 and correspond to the following:

Step I. As in *pathway A*.

Step II. As in *pathway A*. Note that there is reduced surface complex stability due to the crystal field stabilisation of the O^{2-} species, which makes the O_S site less nucleophilic.

Step III. As in *pathway A*. The reduced stability of the CO_2^{2-} surface species, resulting from competition with the crystal field, is again emphasized.

Step IV. The straightening of the charged CO_2 surface species is associated with a concerted electron transfer to the substrate. The resulting interaction between the formed CO_2 and the reduced substrate becomes repulsive and consequently CO_2 is ejected.

Step V. The CO_2 molecule leaves the surface, resulting in an oxygen vacancy and a reduced substrate. The asymptotic stability of the product becomes 1.6 eV, which is less than that of *pathway A*. This reflects the greater initial stability of the O_S^{2-} species than that of O_W^{2-}, due to the different local crystal fields at these sites.

3.3.3. Implications for Co_3O_4(110)-mediated CO oxidation. The resulting stabilities of the intermediates along the two CO oxidation pathways described in Section 3.3.2 are compared in Fig. 11. This illustrates the significant difference expected in the kinetics and thermodynamics depending on which oxygen is removed from the surface structure.

Key observations comprise the following; (a) *pathway A* introduces quasistable CO_2^{2-} surface transients, (b) significant stabilization is seen upon formation of the CO_2(g) + reduced slab product, and (c) *pathway B* produces a less stable reduced substrate. In particular, (b) and (c) imply that the lifetime of the reduced O_S site should be significantly shorter than that of the O_W site, or conversely, the O_S site is expected to dominate the rates of the redox reactions

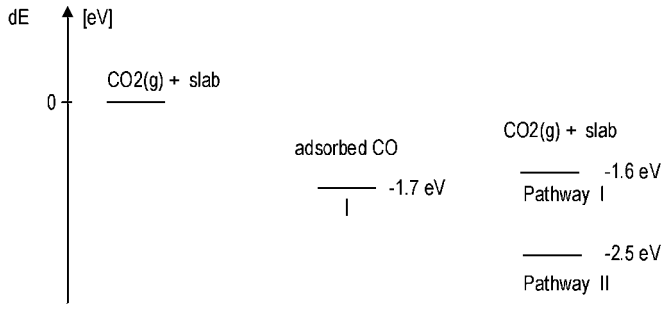

FIG. 11. Comparative exothermicities for paths A and B, relative to the adsorbed CO intermediate at the proposed Co(III) surface site.

associated with the (110) surface of Co_3O_4(s)-mediated oxidation of CO by an oxidant.

4. CONCLUDING REMARKS

First-principles density functional theory calculations have been performed in order to investigate the low-temperature activity of Co_3O_4 for CO oxidation. The calculations, performed on the (110) surface, employed a slab with periodic boundary conditions. The applicability of the computational procedure was verified by comparing the experimentally known structural data for Co_3O_4(s), the isolated CO molecule, and the isolated CO_2 molecule. The theoretical results are accurate to the 2% level.

The previously studied electroneutral Co_3O_4(110) surface was chosen for this CO adsorption investigation. Indeed, our calculations indicate that the (110) surface as obtained by cleaving the bulk structure is quite stable, in that relaxation effects are small.

Three different possible initial CO adsorption sites on the (110) surface were investigated. These correspond to a surface oxygen, a Co(III) ion between two oxygen ions in a subsurface geometry, and a Co(III) ion in the top layer. Results of the calculations imply that the latter site is the only one suitable for initial CO adsorption. Thus, the CO molecule is found to bind with the carbon end to a Co(III) ion on the surface at $R_{Co–C} = 1.8$ Å with a binding energy of 1.7 eV. Calculations, performed on TiO_2, give a binding energy of 0.8 eV for adsorbing CO at a Ti site (21). Furthermore, the adsorption energy for the spinel cobalt oxide is estimated to be about double that value, according to catalytic activity theory (32). The latter estimate is in agreement with the independent 1.7 eV result obtained in the present study.

The initial CO adsorption site at a surface Co(III) ion, determined in the present study, was found to change the ligand field on this ion. This in turn resulted in the ion becoming paramagnetic rather than diamagnetic. This change in surface magnetic property could be used to experimentally validate the nature of the proposed adsorption complex, particularly so since this configuration is not the

same as that discussed in Ref. (16). The latter subsurface candidate site for reactive CO adsorption was ruled out, based on the prohibitively large Pauli repulsion interactions experienced by the CO molecule from the neighbouring surface oxygen ions in the entrance channel.

Starting from the Co(III)–CO surface complex, two reaction paths towards CO oxidation were considered. Indeed, in the proximity of this adsorption site there are two symmetry-inequivalent oxygen ions, both of which could be involved in the oxidation of CO. These two oxygen ions differ in the way they are bound to the lattice, and consequently they experience different crystal fields. Stability changes along the two pathways for O_{surf} abstraction by CO to form CO_2 were computed. While the two pathways produce similar intermediate O_{surf}–CO structures, the computed stabilities deviate significantly. The first three steps are common to both pathways.

1. CO adsorbs on a surface-exposed Co^{3+}.
2. CO glides towards the oxygen, forming a surface CO complex, displaying bonds to both the surface oxygen and the Co(III) site.
3. A charged O_{surf}–CO species is formed with a bent equilibrium structure.

Here, the reactions bifurcate, as the O_{surf} at the strong crystal field site (O_S) does not possess a quasistable linear CO_2^{2-} intermediate structure, while the O_{surf} abstraction from the weak crystal field site (O_W) displays a barrier for linear CO_2^{2-} to CO_2(g) interconversion. Both possibilities eventually reduce the active site.

The two reaction pathways are expected to display different catalytic activities. Specifically, the energy difference between reactants and product is substantially larger for removing the oxygen from the weak crystal field site, i.e., 2.5 eV (O_W) relative to 1.6 eV (O_S). This, in conjunction with substantially stabilized intermediate surface complexes, implies that the O_W site is more reluctant to reoxidize than the O_S surface site. The pathway for the oxygen abstraction from the strong crystal field site displays several additional characteristics, which may be useful in the context of catalysis. One such observation is that only negligible energy difference is obtained when CO_{ads} reacts with O_S to form CO_2, which in conjunction with the significantly faster rate of reoxidation expected for this surface site point to the O_S site as the dominant site in determining the catalytic redox properties of the (110) surface of Co_3O_4(s).

The scenario described above may also be used to explain the loss of activity resulting from the solid-state reaction product between Co_3O_4 and the alumina support whereby $CoAl_2O_4$ is formed. This is in spite of the fact that $CoAl_2O_4$ has the same spinel structure as Co_3O_4. The decisive factor is that in $CoAl_2O_4$, Co and Al assume oxidation states II+ and III+, respectively. Neither one of these ions is likely to be reduced upon surface oxygen abstraction and therefore this compound becomes inactive towards CO(g) oxidation, following the above outlined mechanism, which has an intermediate electron sink as a necessary prerequisite.

In summary, it was demonstrated how oxide materials with significant CO oxidation capacity benefit from having an effective electron sink, e.g., in terms of the reduction of Co^{3+} to Co^{2+} in the Co_3O_4 spinel structure, for harbouring the excess electrons upon CO_2 formation, until being reoxidised by O_2. Two paths for oxygen abstraction were discussed. Future investigations will include (a) calculations to determine activation energies along the outlined reaction paths for kinetics modelling, and (b) addressing other oxide surfaces with possible catalytic capacity by employing the strategy developed here.

ACKNOWLEDGMENTS

The work in this paper has been performed within the Competence Centre for Catalysis, which is financially supported by the Swedish National Energy Administration and the member companies: AB Volvo, Johnson Matthey CSD, Saab Automobile AB, Perstorp AB, MTC AB, Eka Chemicals, and Swedish Space Corporation. Support from the Swedish Research Council (PB, and IP) is gratefully acknowledged, as is constructive discussions with Prof. Bengt Andersson.

REFERENCES

1. Leaners, G., *Sci. Total Environ.* **189/190**, 139 (1996).
2. Rijkeboer, R. C., *Catal. Today* **11**, 141 (1991).
3. Panas, I., and Siegbahn, P., *Chem. Phys. Lett.* **153**, 5 (1988) .
4. Burk, P. L., Hochmuth, J. K., Anderson, D. R., Sung, S., Punke, A., Dahle, U., Tauster, S. J., Tolentino, C. O., Rogalo, J., Miles, G., Mignano, M., and Niejako, M., *Stud. Surf. Sci. Catal.* **96**, 919 (1995).
5. Thormählen, P., Skoglundh, M., Fridell, E., and Andersson, B., *J. Catal.* **188**, 300 (1999).
6. Yao, Y. Yu., *J. Catal*. **33**, 108 (1974).
7. Drago, R. S., Jurczyk, K., Singh, D. J., and Young, V., *Appl. Catal. B* **6**, 155 (1995).
8. Garbowski, E., Guenin, M., Marion, M. C., and Primet, M., *Appl. Catal.* **64**, 209 (1990).
9. Meng, M., Lin, P. Y., and Fu, Y. L., *Catal. Lett.* **48**, 213 (1997).
10. Cunningham, D. A. H., Kobayashi, T., Kamijo, N., and Haruta, M., *Catal. Lett.* **25**, 257 (1994).
11. Boreskov, G. K., *in* "Catalysis: Science and Technology" (J. R. Andersson and M. Bourdart, Eds.), Vol. 3, p. 39. Springer-Verlag, Berlin, 1982.
12. Shelef, M., Otto, K., and Gandhi, H., *J. Catal.* **12**, 361 (1968).
13. Jansson, J., *J. Catal.* **194**(1), 55 (2000).
14. Mars, P., and van Krevelen, D. W., *Chem. Eng. Sci.* **3**(Suppl.), 41 (1954).
15. Ziólkowski, J., and Barbaux, Y., *J. Mol. Catal.* **67**, 119 (1991).
16. Iwasawa, Y., *Adv. Catal.* **35**, 8822 (1987).
17. Kohn, W., and Sham, L. J., *Phys. Rev*. **140**, 1133 (1965).
18. Perdew, J. P., Burke, K., and Ernzerhof, M., *Phys. Rev. Lett.* **77**(18), 3865 (1996).
19. Payne, M. C., Teter, M. P., Allan, D. C., Arias, T. A., and Joannopoulus, J. D., *Rev. Mod. Phys.* **64**(4) 1045 (1992).
20. Cerius^2 available from Accelrys, formerly Molecular Simulations, Inc.
21. Monkhorst, H. J., and Pack, J. D., *Phys. Rev. B* **13**, 5188 (1976).
22. Sorescu, D. C., and Yates, J. T., *J. Phys. Chem. B* **102**, 4556 (1998).
23. Vanderbilt, D., *Phys. Rev. B* **41**(11), 7892 (1990).
24. Fischer, T. H., and Almlöf, J., *J. Phys. Chem.* **96**, 9768 (1992).

25. Knop, O., Reid, K. I. E., Sutaru, O., and Nakagawa, Y., *Can. J. Chem.* **46**, 3463 (1968).
26. Lide, D. R., Ed., "CRC Handbook of Chemistry and Physics," 73rd ed. CRC Press, Boca Raton, FL, 1992–1993.
27. Becke, A. D., *J. Chem. Phys.* **98**, 5648 (1993).
28. Lee, C., Yang, W., and Parr, R. G., *Phys. Rev. B* **37**, 785 (1988).
29. Vosko, S. H., Wilks, L., and Nusair, M., *Can. J. Phys.* **58**, 1200 (1980).
30. Frisch, M. J., Trucks, G. W., Schlegel, H. B., Scuseria, G. E., Robb, M. A., Cheeseman, J. R., Strain, M. C., Burant, J. C., Stratmann, R. E., Dapprich, S., Kudin, K. N., Millam, J. M., Daniels, A. D., Petersson, G. A., Montgomery, J. A., Zakrzewski, V. G., Raghavachari, K., Ayala, P. Y., Cui, Q., Morokuma, K., Foresman, J. B., Cioslowski, J., Ortiz, J. V., Barone, V., Stefanov, B. B., Liu, G., Liashenko, A., Piskorz, P., Chen, W., Wong, M. W., Andres, J. L., Replogle, E. S., Gomperts, R., Martin, R. L., Fox, D. J., Keith, T., Al-Laham, M. A., Nanayakkara, A., Challacombe, M., Peng, C. Y., Stewart, J. P., Gonzalez, C., Head-Gordon, M., Gill, P. M. W., Johnson, B. G., and Pople, J. A, Gaussian98, Gaussian, Inc., Pittsburgh, PA, 1998.
31. Roth, W. L., *J. Phys. Chem. Solids* **25**, 1 (1964).
32. Atkins, P. W., "Physical Chemistry," 6th ed. Oxford Univ. Press, Oxford, 1998.